Supporting Information

Vertically-stacked MXene/rGO composite membrane for highly efficient H_2/CO_2 separation

Zhaorui Dong[a,1], Yiyi Fan[a,1], Xiuxia Meng[a,*] Yun Jin[a], Jian Song[a], Xiaobin Wang[a], Naitao Yang[a,*], Jaka Sunarso[b,*], Shaomin Liu[c]

[a]School of Chemistry and Chemical Engineering, Shandong University of Technology, Zibo 255049, P.R. China

[b]Research Centre for Sustainable Technologies, Faculty of Engineering, Computing and Science, Swinburne University of Technology, Jalan Simpang Tiga, 93350 Kuching, Sarawak, Malaysia

[c]State Key Laboratory of Separation Membranes and Membrane Processes, Department of Chemical Engineering, Tiangong University, Tianjin 300387, P.R. China

[1]These authors contributed equally to this work. *Corresponding authors. E-mail addresses: mengxiux@sdut.edu.cn (X. Meng), naitaoyang@126.com (N. Yang), barryjakasunarso@yahoo.com, jakasunarso@swinburne.edu.my (J. Sunarso)

Experimental

Preparation of $Ti_3C_2T_x$ and GO nanosheets

$Ti_3C_2T_x$ nanosheets were obtained by selectively removing the Al atom layer from the corresponding MAX (Ti_3AlC_2) precursor using a mild etching. Firstly, 1 g of Ti_3AlC_2 powder (purchased from Laizhou Kai Ceramic Materials) was slowly added into hydrochloric acid (HCl, 20 mL, 6 M) and lithium fluoride (LiF, 1 g) solution mixture at 45 °C for 24 h under magnetic stirring. Subsequently, the reacted slurry was centrifuged and washed with deionized (DI) water at 7000 rpm until the pH of the supernatant became higher than 6. Lastly, the sediment was dispersed into DI water (80 mL) under 1 h of sonication and 10 min of low-speed centrifugation to remove unexfoliated MXene. The obtained $Ti_3C_2T_x$ colloidal solution with a concentration of 12 mg mL^{-1} was collected in a glass bottle. The graphene oxide (GO) nanosheets were prepared from graphite using the modified Hummers method.[1] The concentration of stable GO nanosheet aqueous dispersion was about 12 mg mL^{-1}.

Fabrication of vertical MXene/rGO composite membrane

MXene/rGO composite membrane was fabricated *via* reduction of Zn foil combining physical cutting-reassemble method (**Fig. 1**). The obtained MXene colloidal solution was slowly added into GO dispersion to form MXene/GO aqueous dispersion under 1 hour of violent stirring in an argon atmosphere. Subsequently, MXene/rGO composite membranes were obtained using reduction of Zn foil for 1 hour. The above membrane was peeled off from the Zn foil by immersing it into a 1 M H_2SO_4 solution to obtain free-standing MXene/rGO composite membranes. After that, the composite membrane was repeatedly washed with DI water and then freeze-dried for 4 hours to obtain MXene/rGO composite membrane. The GO content was adjusted by different volumes or concentrations of GO aqueous dispersion. The mass ratio of MXene to GO was 1, 2, and 3 in the MXene/GO solution mixture, labelled as 1-MXene/rGO, 2-MXene/rGO, and 3-MXene/rGO, respectively. To obtain the vertical and horizontal composite

membranes, a physical cutting-reassembly method was used under different orientations.

Gas permeance test of MXene/rGO composition membrane

The obtained MXene/rGO composite membrane was tested in a homemade permeation cell to measure its separation performance for either single-gases or their mixtures (**Figure S12**). The effective membrane area is 0.03 cm^2 in testing. To avoid the leakage of gas, epoxy glue was used to seal the membrane. The flow rate of the permeated single gas was measured at room temperature using a bubble flow meter. In the case of gas mixtures, permeance and selectivity or separation factor were calculated as described in our previous work.[2] H_2 and another gas, i.e., CO_2, N_2, or CH_4 with a volume ratio of 1:1 were used as the feed gas. The total flow rate was set at 60 mL min^{-1}. On the other hand, argon with a flow rate of 60 mL min^{-1} was used as a sweep gas at atmospheric pressure. Gas composition on the sweep side was measured using an online gas chromatograph (7890B, Agilent) with thermal conductivity detector. The selectivity or separation factor was calculated as the average of three measurements (triplicates) under steady-state.

Characterization of MXene nanosheets and membranes

The surface morphologies of $Ti_3C_2T_x$ (MXene), GO, and MXene/rGO composite membranes were characterized using field emission scanning electron microscopy (SEM, FEI Aprreo S, Thermofisher) and transmission electron microscopy (TEM, Titan) with an accelerating voltage of 200 kV. The phase information were determined by powder X-ray diffraction and in-situ XRD (XRD, Bruker D8 Advance, Germany) using Cu-Kα radiation (λ = 0.15404 nm) at 2θ range of 5–80° with a step size of 0.02° and a scan rate of 2° min^{-1}. Surface functional groups of MXene, MXene/GO powers, and MXene/rGO composition membranes were characterized using Fourier transform infrared spectrometer (FTIR, Nicolet 5700, United States). The surface roughness

profiles of MXene and GO membranes were characterized using an atomic force microscope (AFM, XE-100, Korea). The Raman spectra were recorded by a spectrophotometer (DXR, Thermo-Fisher Scientific) with an operating wavelength of 532 nm. The chemical states of the surface species were identified using X-ray photoelectron spectroscopy (XPS, 95Perkin Elmer PHI 1600).

Mathematical model derivation

To explain and understand the experimental results, we conceptualized two membrane structures with different nanochannels arrangements, i.e., (i) horizontally stacked and (ii) vertically arranged interlayer spaces for gas diffusion (**Figure S1**). The mathematical models of the gas transport mechanism in the MXene/rGO layered membranes with two different nanochannels arrangements was developed.

In our model, H_2 with a kinetic diameter of 2.89 Å and CO_2 with a kinetic diameter of 3.30 Å diffused through the MXene/rGO layered membrane. In horizontally stacked layered membrane, transport nanochannels are composed of interlayer spacing (3.41 Å) between stacked MXene sheets and randomly distributed nanoscale wrinkles. In the vertically arranged layered membrane, the interlayer spacing is the main transport nanochannels. Accordingly, the size of the transport nanochannels is comparable to the kinetic diameter of the gas molecule. Knudsen diffusion (Kn) and molecular sieving (MS) gas transport model was applied to the MXene/rGO layered membrane. The following assumptions were used:

(1) One-dimensional transport model was used.

(2) Two different transport nanochannels were present, i.e., (i) horizontally stacked and (ii) vertically arranged interlayer spaces (**Figure S1**). Their size remains unchanged with a variation in temperature.

(3) The MXene/rGO layered membrane operated at a steady-state, isothermal condition.

(4) The ideal gas model was applicable to H_2 and CO_2 transports and the actual selectivity can be approximated by the ideal selectivity.

Consequently, Knudsen diffusion and molecular sieving both contribute to total mass movement. **Equation (S1)** can be used to write the total permeance as follows:

$$P_{total} = P_{Kn} + P_{MS} \tag{S1}$$

Here, F_{total}, F_{Kn}, and F_{MS} stand for the total gas permeance, the permeance contributed by Knudsen diffusion, the permeance resulting from molecular sieving, respectively. Typically, the diffusion flux (J_i) for gas can be presented in terms of pressure gradient by Fick's first law as **Equation (S2)**.

$$J_i = -\varphi D \frac{dc}{dz} = -\frac{\varphi D}{RT}\frac{dP}{dz} \tag{S2}$$

where **Equation (S5)** gives the factor for geometrical effects of structure, denoted as φ. The absolute temperature (K) and the ideal gas constant (J mol^{-1} K^{-1}) are denoted by T and R, respectively. D is the diffusion coefficient (molecular sieving and Knudsen diffusion). The expression for D in Knudsen diffusion is **Equation (S3)**.

$$D_{Kn,i} = \frac{d_p}{3}\left(\frac{8RT}{\pi M}\right)^{\frac{1}{2}} \tag{S3}$$

where M and d_p stand for the diffusing gas's molecular weight (kg mol^{-1}) and diffusion pore diameter (3.41 Å), respectively. **Equation (S4)** is the formula for the Knudsen diffusion flux ($J_{K,i}$) that is generated by combining **Equation (S2)** and **(S3)**.

$$J_{Kn,i} = -\frac{\varphi d_p}{3}\left(\frac{8}{\pi MRT}\right)^{\frac{1}{2}}\frac{dP}{dz} \tag{S4}$$

$$\varphi = \frac{\varepsilon}{\tau} = \frac{(1-\frac{a}{d})}{\tau} \tag{S5}$$

where ε, a, and d stand for the membrane porosity, the thickness of the monolayer MXene nanosheet (~10 Å), the d-spacing (~13.4 Å), respectively.

The tortuosity factor (τ) was introduced for the membrane structure analysis, which can be approximated as the ratio of the diffusion length (l_s) to the membrane thickness (δ), represented by **Equations (S6)**.

$$\tau = \frac{l_s}{\delta} \tag{S6}$$

The Knudsen diffusion permeance through MXene/rGO composite membrane can be calculated by **Equations (S7)**.

$$P_{Kn,i} = \frac{J_K}{\Delta P} = \frac{\varepsilon d_p}{3 l_s} \left(\frac{8}{\pi M R T}\right)^{\frac{1}{2}} \quad \text{(S7)}$$

As such, molecular sieving model (MS) can be derived using the kinetic theory of gases.[3] The molecular sieving flux can be expressed in terms of the pressure gradient whereby the MS flux ($J_{M,i}$) is expressed as **Equation (S8)**.

$$J_{M,i} = - D_{M,i} \frac{dc}{dz} = - \frac{D_{M,i} d_p}{RT\ dz} \quad \text{(S8)}$$

where $D_{M,i}$ ($m^2\ s^{-1}$) is the molecular sieving coefficient of the MXene/rGO layered membrane, which was modified from the earlier model[4] and is shown as **Equation (S9)**.

$$D_{M,i} = \frac{1}{Z l_s} \left(\frac{8RT}{\pi M}\right)^{\frac{1}{2}} exp\left(-\frac{E_a}{RT}\right) \quad \text{(S9)}$$

where Z, l_s, R, T, and M are the number of adjacent sites, the diffusion length (m), the gas constant ($J\ mol^{-1}\ K^{-1}$), the operating temperature (K), and the molecular weight ($kg\ mol^{-1}$), respectively. E_a is the activation energy of gas diffusion ($kJ\ mol^{-1}$), which is required for the molecule to surmount the attractive constrictions imposed by the nanochannels structure. The molecular sieving flux ($J_{M,i}$, $mol\ m^{-2}\ s^{-1}$) is obtained by combining **Equations (S8)** and **(S9)**, as shown by **Equation (S10)** below.

$$J_{M,i} = - \frac{1}{Z l_s} \left(\frac{8}{\pi M R T}\right)^{\frac{1}{2}} exp\left(-\frac{E_a}{RT}\right) \frac{dp}{dz} \quad \text{(S10)}$$

The gas permeance from MS through a microporous membrane is obtained after integrating **Equation (S10)** over the membrane thickness δ (m), giving **Equation (S11)**.

$$P_{M,i} = \frac{J_{M,i}}{\Delta p} = \frac{1}{Z l_s \delta} \left(\frac{8}{\pi M R T}\right)^{\frac{1}{2}} exp\left(-\frac{E_a}{RT}\right) \quad \text{(S11)}$$

Equation (S11) reveals an exponential dependence of the gas permeance on the temperature. H_2 and CO_2 permeances through MXene/rGO layered membrane under different temperatures were evaluated to obtain Arrhenius plot for the calculation of the activation energy of gas diffusion.

To investigate the effects of tortuosity factor on gas permeance through MXene/rGO membrane, **Equations (S11)** and **(S6)** can be combined to give **Equation (S12)** as follows:

$$P_{M,i} = \frac{1}{Z \tau \delta^2} \left(\frac{8}{\pi M R T}\right)^{\frac{1}{2}} exp\left(-\frac{E_a}{RT}\right) \quad \text{(S12)}$$

Figures

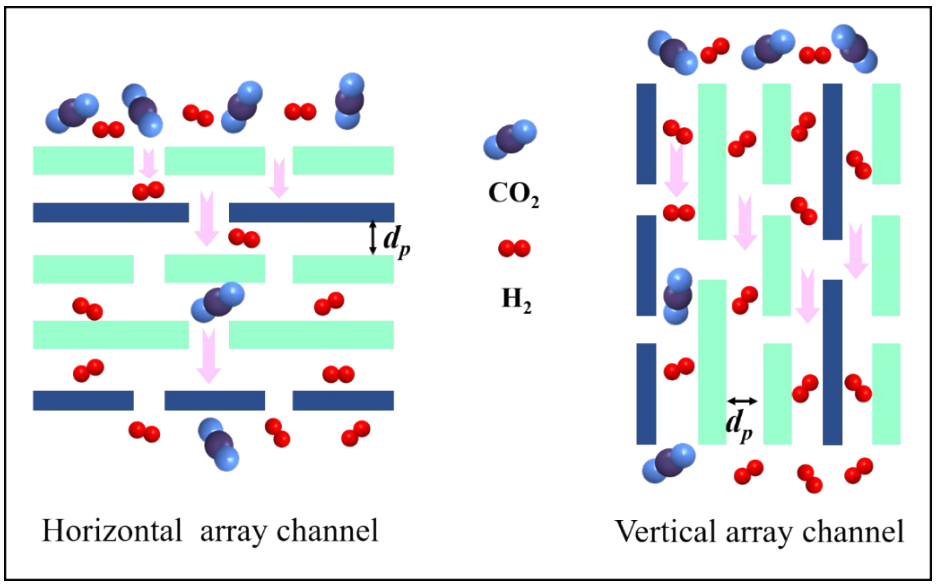

Figure S1. Schematic illustration of the two different 2D membrane structures with **(left)** horizontally stacked and **(right)** vertically arranged interlayer spaces for gas diffusion.

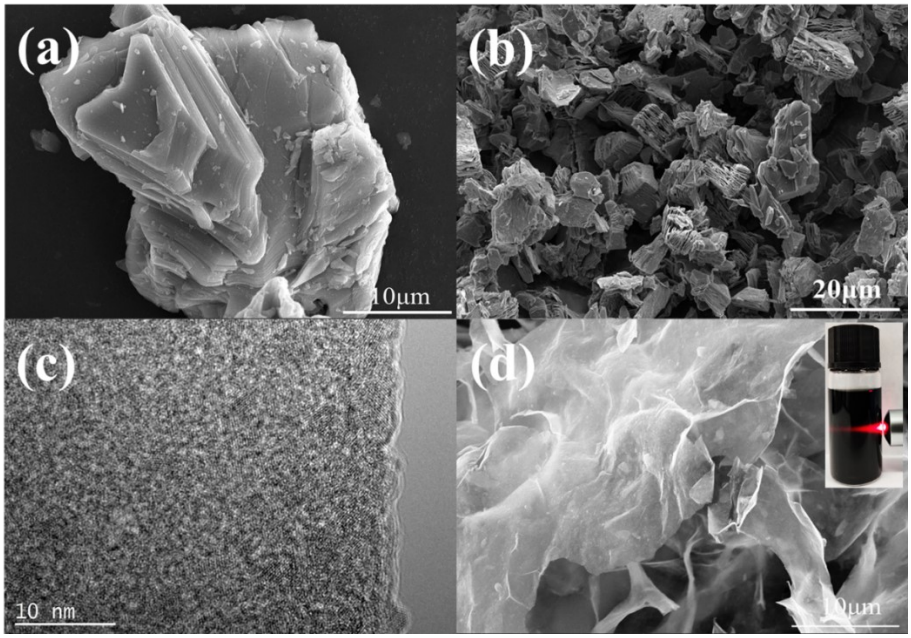

Figure S2. SEM image of **(a)** Ti_3AlC_2, **(b)** $Ti_3C_2T_x$. **(c)** HRTEM image of $Ti_3C_2T_x$ nanosheet. **(d**) SEM image of MXene/GO composite nanosheets (2-MXene/GO) (**Inset**: stable colloidal solution).

Note: $Ti_3C_2T_x$ (MXene) nanosheets were obtained after the selective removal of Al layers from the corresponding MAX precursor (Ti_3AlC_2, **Figure S2(a)**) using mild LiF and HCl etching solution mixture (**Figure S2(b)**). After sonication and centrifugation, the MXene could be delaminated to monolayer nanosheets, forming a stable colloidal solution in water.

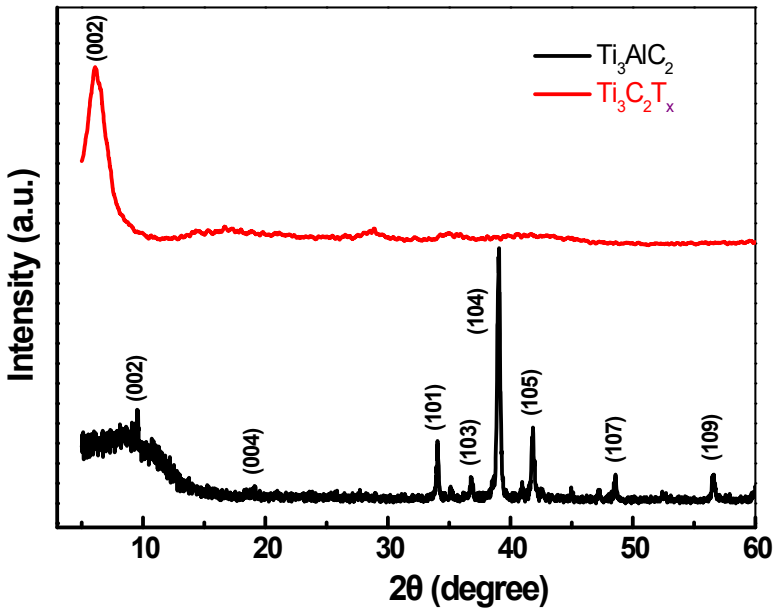

Figure S3. Powder XRD patterns of Ti_3AlC_2 and $Ti_3C_2T_x$ powders.

Note: The characteristic diffraction peak for the (104) planes of Ti_3AlC_2, which should be located at 2θ of 39°, was absent on the powder XRD pattern of $Ti_3C_2T_x$ (**Figure S3**), which indicates that the Al layers were removed by the solution mixture. This is consistent with previous literature results.[5] Additionally, the (002) peak shifted toward a lower 2θ value, which suggested that the accordion-like $Ti_3C_2T_x$ formed after the etching of the Al atomic layer.

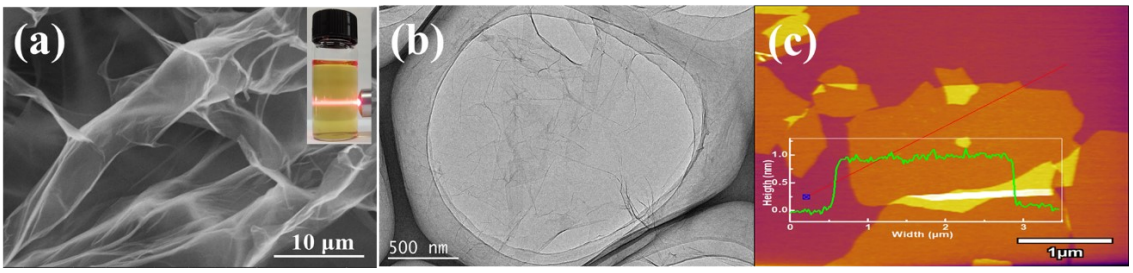

Figure S4. (a) SEM image of GO sheets (**Inset:** stable colloidal solution); **(b)** High-resolution TEM image of GO nanosheets; **(c)** AFM profile of GO nanosheets.

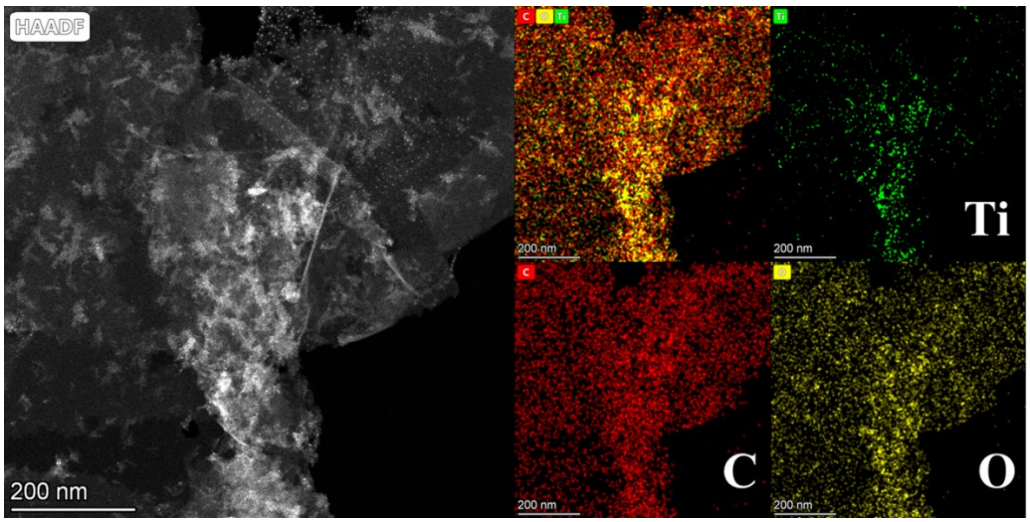

Figure S5. HAADF-STEM mapping images of MXene/GO composite nanosheets.

Note: The distribution of Ti, C, and O elements is shown in the mapping images of the MXene/GO composite nanosheets. Ti, C, and O elements are uniformly spread, further demonstrating the uniform mixing of MXene and GO sheets.

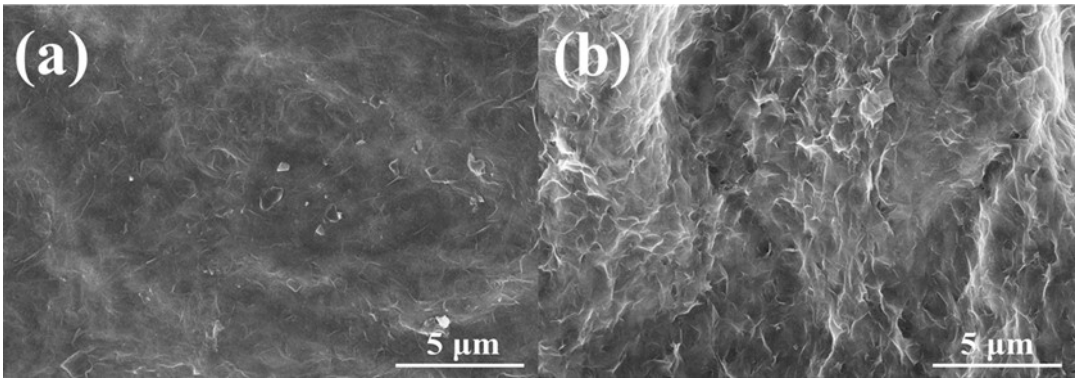

Figure S6. SEM images of the (a) inner surface; (b) outer surface of 2-MXene/rGO composite membrane.

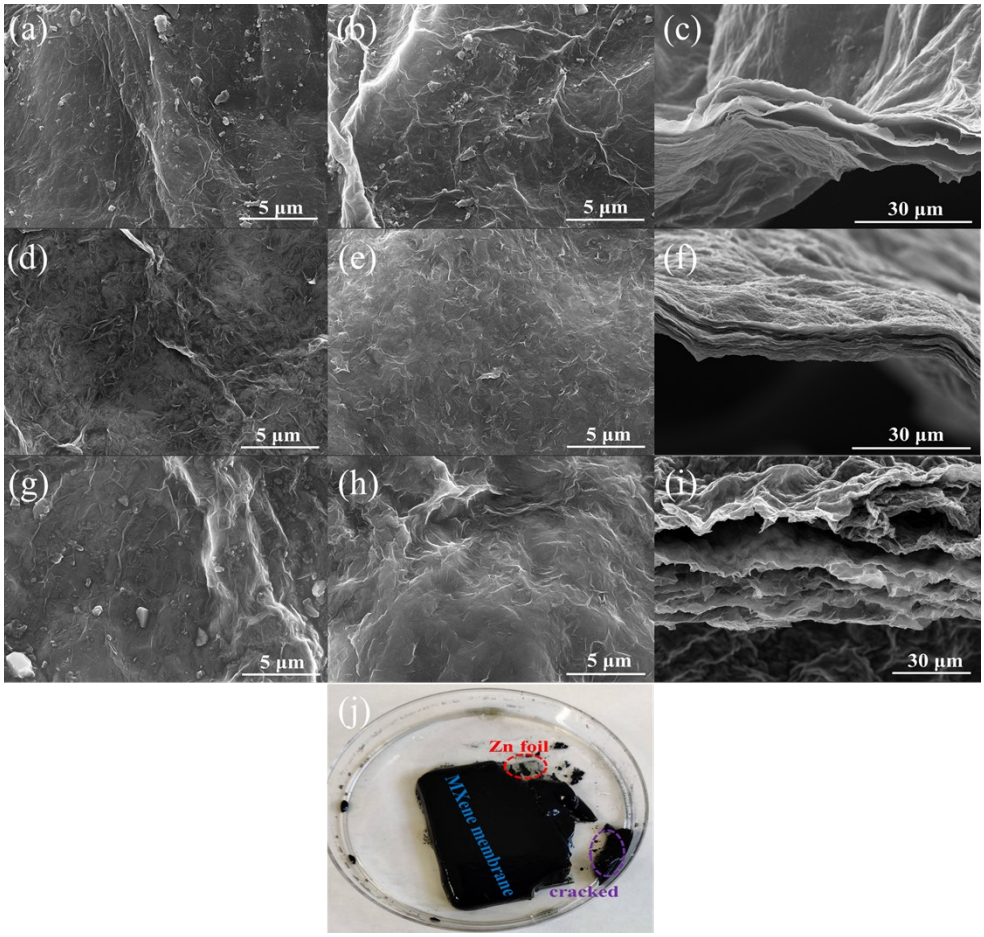

Figure S7. SEM images of **(a, d, g)** the inner surface; **(b, e, h)** the outer surface; and **(c, f, i)** the cross-section for **(a, b, c)** rGO; **(d, e, f)** 1-MXene/rGO; and **(g, h, i)** 3-MXene/rGO membranes; **(j)** Digital photograph of the MXene membrane was prepared by zinc foil reduction.

Note: Due to the addition of large GO nanosheets, the obtained MXene/rGO composite membrane exhibits a continuous and laminar structure. With the decrease of GO concentration in colloidal solution, the outer surface of the MXene/rGO composite membrane becomes rougher, similar to the MXene membrane. The MXene membrane without GO content was easily destroyed after peeled-off from the Zn foil given the weak binding force between MXene nanosheets, highlighting the beneficial role of flexible GO.

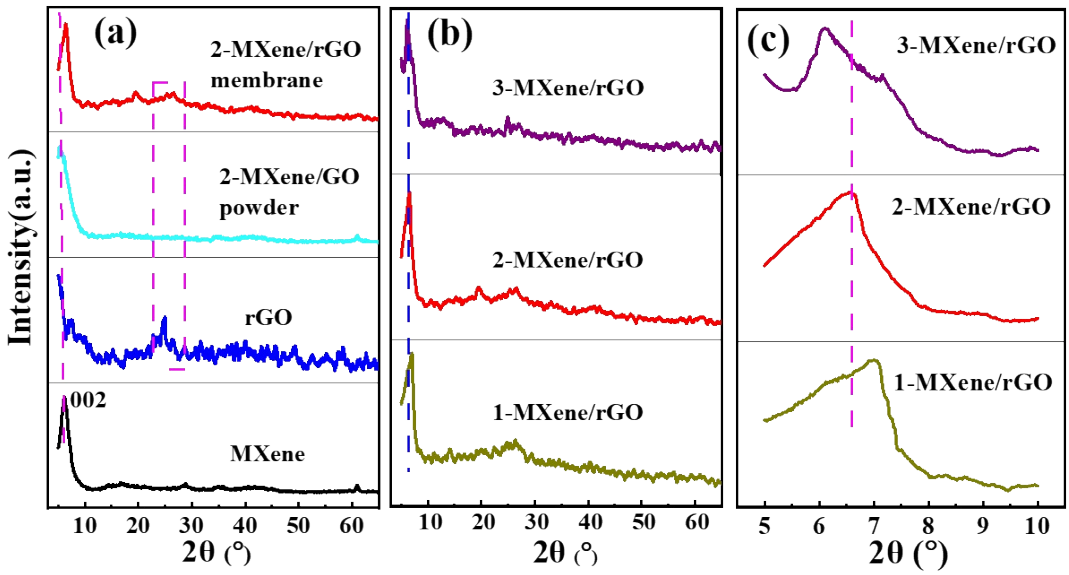

Figure S8. (a) Powder XRD patterns of MXene sheets, rGO sheets, 2-MXene/GO powder, and 2-MXene/rGO membrane; **(b)** Powder XRD patterns of **(bottom)** 1-MXene/rGO; **(center)** 2-MXene/rGO; and **(upper)** 3-MXene/rGO; **(c)** Magnified portion of the patterns of 1-MXene/rGO, 2-MXene/rGO, and 3-MXene/rGO membranes at 2θ of 5-10°.

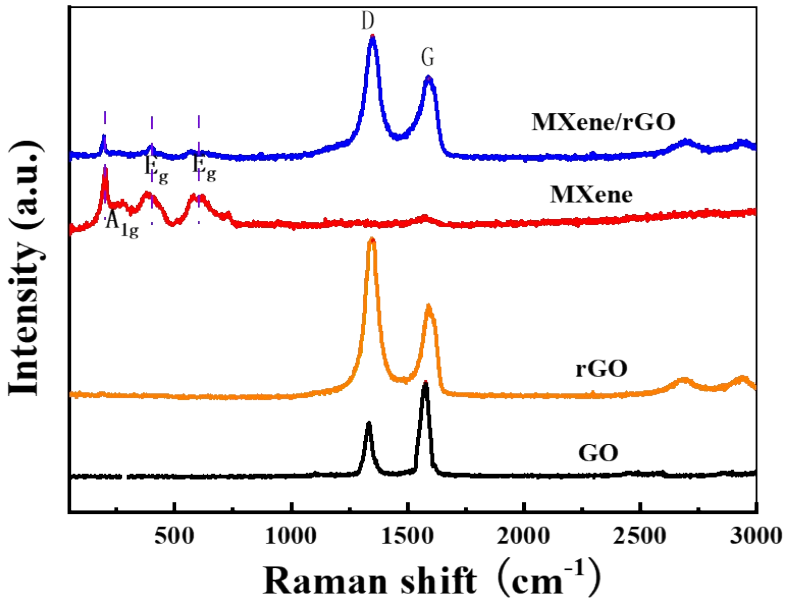

Figure S9. Raman spectra of GO sheets, rGO sheets, MXene sheets, and 2-MXene/rGO membrane.

Note: The similar features on the Raman spectra profiles for the MXene sheets and MXene/rGO composite membrane at the Raman shift range of 150-750 cm^{-1} came from the vibrations of Ti and C surface functional groups.[6, 7] The characteristic peaks of rGO sheets at Raman shift of 1348 and 1591 cm^{-1} also appear on the profile for the MXene/rGO membrane, which confirms the presence of rGO sheets in this membrane. These peaks can be assigned to the D and G bands of the local defects/disorders and the ordered sp2 graphitic carbon, respectively.[8, 9] In comparison to the pure GO sheets, the higher ratio of the intensity of the D band to that of the G band (I_D/I_G ratio) for the MXene/rGO membrane indicates the successful reduction of GO to rGO by the Zn foil. Moreover, the slight shift by 14 cm^{-1} of the location of the G band of MXene/rGO membrane (at Raman shift of 1591 cm^{-1}) relative to that of the pure GO (at Raman shift of 1577 cm^{-1}) was likely caused by the formation of Ti-O-C bonds between MXene and rGO.

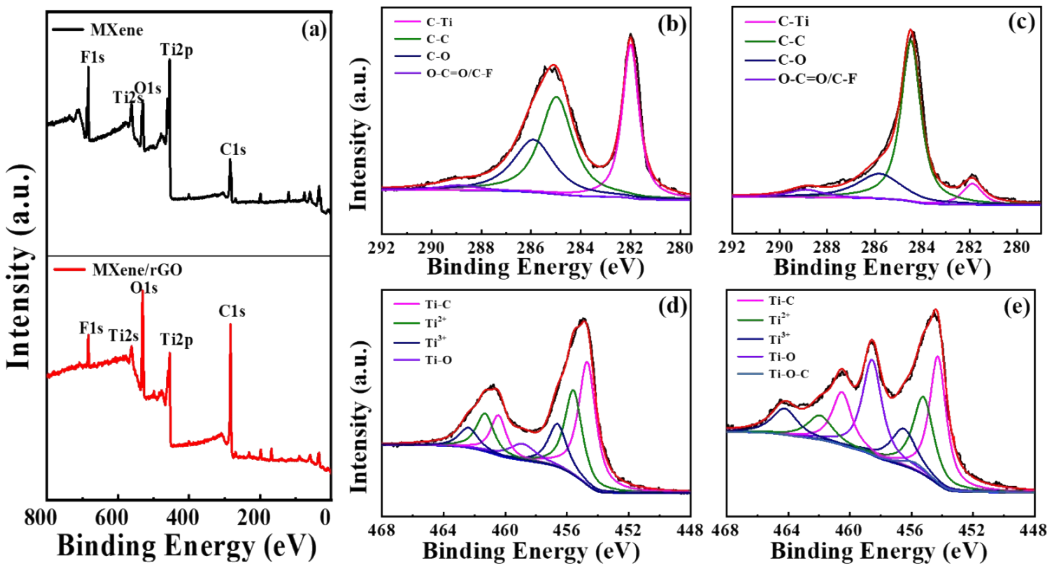

Figure S10. The XPS spectra of the MXene sheets and 2-MXene/rGO membrane. **(a)** Survey scan spectra of **(upper)** MXene sheets and **(bottom)** 2-MXene/rGO membrane; C 1s spectra of **(b)** MXene sheets and **(c)** 2-MXene/rGO membrane; Ti 2p spectra of **(d)** MXene sheets and **(e)** 2-MXene/rGO membrane.

Note: The XPS survey scan spectra indicate that 2-MXene/rGO membrane were mainly composed of C, Ti, O, and F. In comparison to the C 1s spectrum of MXene, the intensity of the C-Ti peak was reduced while that of the C-C peak was increased for the C 1s spectrum of MXene/rGO membrane. The C-O peak at the binding energy of 286 eV of the MXene/rGO membrane was also reduced relative to that of MXene. These denote the reduction of GO during the assembly process. Furthermore, on the Ti 2p spectrum of MXene/rGO membrane, a new Ti-O-C peak appears at the binding energy of 455.8 eV, which came from the covalent bonding between MXene and rGO nanosheets.[10]

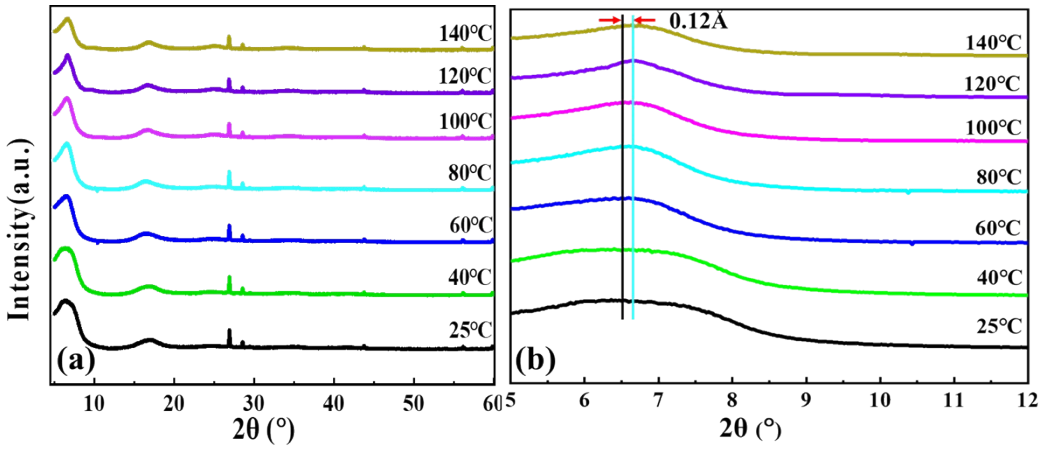

Figure S11. (a) *In situ* powder XRD patterns of the 2-MXene/rGO membrane; **(b)** Magnified portion of the patterns at 2θ of 5-12°.

Note: The interlayer spacing of 2-MXene/rGO was observed at temperature range of 20-140 °C. $Ti_3C_2T_x$ (MXene) and rGO have abundant functional groups on theirs surfaces and edges.[11, 12] With temperature rise, the de-functionalization, i.e., removal of hydroxyl (-OH) groups occurred within the MXene/rGO membrane, which led to the reduction in the interlayer spacing.[2] The interlayer spacing decreased by approximately 0.12 Å as the temperature increased from 20 to 120 °C.

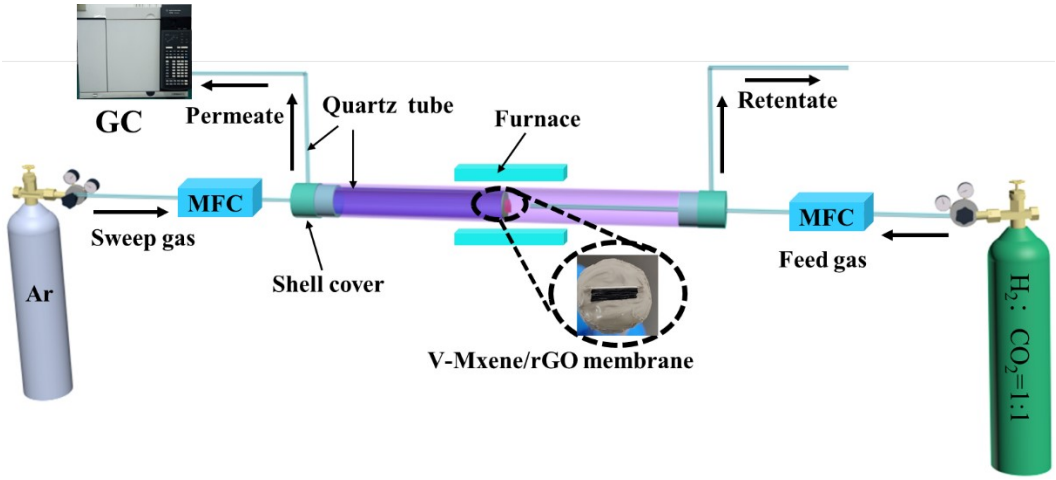

Figure S12. Schematic diagram of the custom-made device for gas mixture permeability test of the MXene/rGO composite membrane.

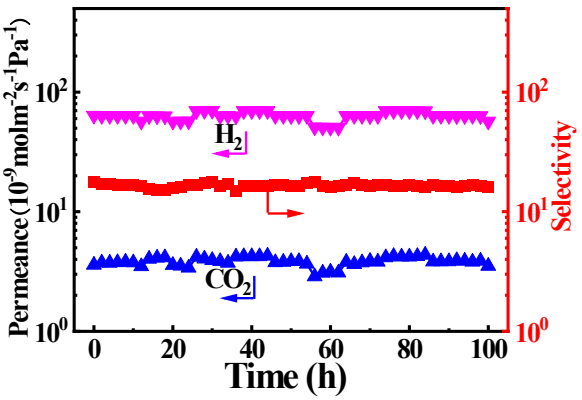

Figure S13. 100-hour continuous permeance and selectivity test result for H_2/CO_2 separation of H-MXene/rGO membrane based on 2-MXene/rGO at room temperature.

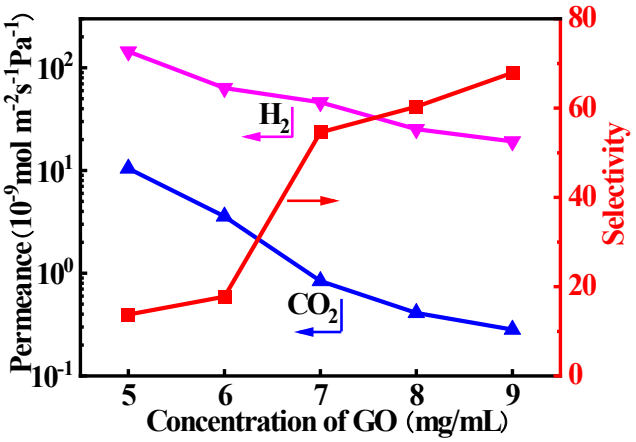

Figure S14. H_2 and CO_2 permeances and H_2/CO_2 selectivities of H-MXene/rGO membrane based on 2-MXene/rGO at room temperature as a function of the concentration of GO in the solution during synthesis.

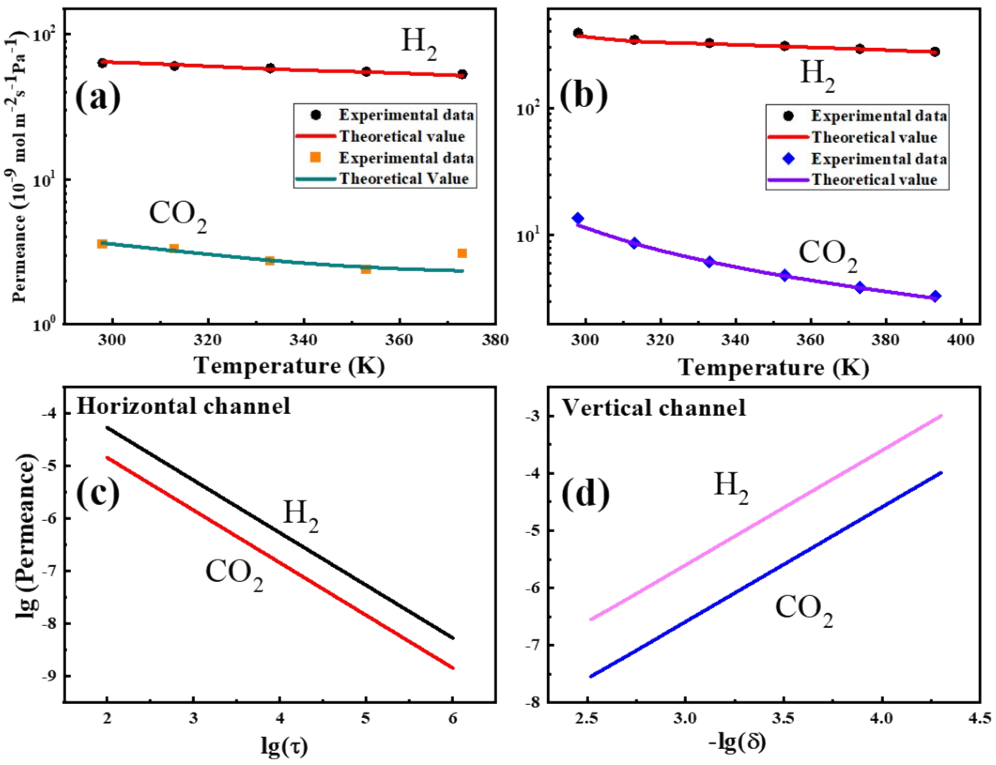

Figure S15. Experimental and simulation results of temperature-dependent H_2 and CO_2 permeances of **(a)** H-MXene/rGO membrane between 298 and 373 K (25 and 100 °C); **(b)** V-MXene/rGO membrane between 298 and 393 K (25 and 120 °C); **(c)** Logarithmic plot of H_2 and CO_2 permeances versus tortuosity factor (τ) for H-MXene/rGO membrane; and **(d)** Logarithmic plot of H_2 and CO_2 permeances versus membrane thickness (l_s) for V-MXene/rGO membrane.

Note: Gas permeance for MS may be computed using **Equations (S1)** and **(S7)**. We then used MATLAB 7.0.1's ordinary least squares approach for regression to get the activation energies of gas diffusion (Ea) in **Equation (S11)**. The resulting model **(Figure S15(b))** with the given parameters suited the experimental results of gas permeance across the V-MXene/rGO membrane well. This resulted in a determination coefficient (R^2) of 0.9966. H_2 and CO_2 permeance were found to have activation energies (Ea) of 62.95 and 65.53 kJ mol^{-1}, respectively. The H-MXene/rGO membrane's diffusion length (l_s) was determined using the same activation energy (Ea) as the V-MXene/rGO membrane, and the result was 0.41 m. As a result, 1.78×104 times

longer diffusion length exists than membrane thickness for H-MXene/rGO. We got the findings presented in (Figure S16(a)) by utilizing these regressed parameters for the gas permeance simulations, and compared the model predictions of gas permeance across H-MXene/rGO membrane with the experimental data. The gas permeance testing data over the H-MXene/rGO membrane were well-fitted by the model results **(Figure S15(a))**.

The aforementioned findings indicate that gas permeance is significantly influenced by the tortuosity factor (τ). According to the current findings, the tortuosity factor (τ) for the V-MXene/rGO membrane is approximately 1. Furthermore, in the current work, the tortuosity factor τ in the H-MXene/rGO membrane was calculated to be approximately 1.78×10^{4} **(Figure S15(c))**. As the maximum gas permeance is obtained for V-MXene/rGO membrane, it suggests that the smaller tortuosity factor of MXene/rGO membrane can lead to higher gas permeance.

However, in the case of the V-MXene/rGO membrane, decreasing the membrane thickness results in a notable improvement in gas permeance **(Figure S15(d))**. Since the square membrane thickness and the gas permeance are inversely correlated, we believe that lowering the membrane thickness is a good way to increase gas permeance even further.

Table

Table S1. The d-spacing and interlayer spacing values for 1-MXene/rGO, 2-MXene/rGO, and 3-MXene/rGO.

	1-MXene/rGO	2-MXene/rGO	3-MXene/rGO
2θ (°)	7	6.58	6.1
d-spacing (Å)	12.61	13.41	14.47
Interlayer spacing (Å)	2.61	3.41	4.47

References

1. J. Cao, C. Chen, K. Chen, Q. Lu, Q. Wang, P. Zhou, D. Liu, L. Song, Z. Niu and J. Chen, *Journal of Materials Chemistry A*, 2017, **5**, 15008-15016.

2. Y. Fan, L. Wei, X. Meng, W. Zhang, N. Yang, Y. Jin, X. Wang, M. Zhao and S. Liu, *Journal of Membrane Science*, 2019, **569**, 117-123.

3. H. Li, Z. Song, X. Zhang, Y. Huang, S. Li, Y. Mao, H. J. Ploehn, Y. Bao and M. Yu, *Science*, 2013, **342**, 95-98.

4. P. F. Lito, S. P. Cardoso, A. E. Rodrigues and C. M. Silva, *Separation & Purification Reviews*, 2014, **44**, 283-307.

5. L. Ding, Y. Wei, L. Li, T. Zhang, H. Wang, J. Xue, L. X. Ding, S. Wang, J. Caro and Y. Gogotsi, *Nat Commun*, 2018, **9**, 155.

6. M. Boota, B. Anasori, C. Voigt, M. Q. Zhao, M. W. Barsoum and Y. Gogotsi, *Adv Mater*, 2016, **28**, 1517-1522.

7. J. Yan, C. E. Ren, K. Maleski, C. B. Hatter, B. Anasori, P. Urbankowski, A. Sarycheva and Y. Gogotsi, *Advanced Functional Materials*, 2017, **27**.

8. S. Xu, G. Wei, J. Li, W. Han and Y. Gogotsi, *Journal of Materials Chemistry A*, 2017, **5**, 17442-17451.

9. Z. Wang, Y. Chen, M. Yao, J. Dong, Q. Zhang, L. Zhang and X. Zhao, *Journal of Power Sources*, 2020, **448**.

10. T. Zhou, C. Wu, Y. Wang, A. P. Tomsia, M. Li, E. Saiz, S. Fang, R. H. Baughman, L. Jiang and Q. Cheng, *Nature Communications*, 2020, **11**.

11. A. Feng, Y. Yu, Y. Wang, F. Jiang, Y. Yu, L. Mi and L. Song, *Materials & Design*, 2017, **114**, 161-166.

12. H. S. Song, M. G. Park, W. Ahn, S. N. Lim, K. B. Yi, E. Croiset, Z. Chen and S. C. Nam, *Chemical Engineering Journal*, 2014, **253**, 264-273.